Applied Catalysis B: Environmental 194 (2016) 157–168

Contents lists available at ScienceDirect

Applied Catalysis B: Environmental

journal homepage: www.elsevier.com/locate/apcatb

Synthesis of novel 2D-2D p-n heterojunction BiOBr/$La_2Ti_2O_7$ composite photocatalyst with enhanced photocatalytic performance under both UV and visible light irradiation

Yanhui Ao*, Kedan Wang, Peifang Wang*, Chao Wang, Jun Hou

Key Laboratory of Integrated Regulation and Resource Development on Shallow Lakes, Ministry of Education, College of Environment, Hohai University, Nanjing, 210098, China

ARTICLE INFO

Article history:
Received 21 November 2015
Received in revised form 19 April 2016
Accepted 25 April 2016
Available online 30 April 2016

Keywords:
p-n heterojunction
$La_2Ti_2O_7$
BiOBr
Photocatalysis

ABSTRACT

In the present work, an efficient composite photocatalyst composed of 2D BiOBr nanoplates and 2D $La_2Ti_2O_7$ thin nanosheets was synthesized. The photocatalytic performance of the as-obtained samples was investigated by the degradation of dye Rhodamine B and phenol under both UV and visible light irradiation. The results demonstrated that the $La_2Ti_2O_7$ modified with proper amount of BiOBr nanosheets exhibited high efficiency in the photocatalytic process, and the holes took part in the photo-decomposition reaction as the main radicals. The morphology, crystallization, photo-response and electrochemical properties of the obtained catalysts were characterized to understand the mechanism of high photocatalytic activity. The results illustrated that the high photocatalytic performance could be ascribed to the following reasons. First of all, the decoration of BiOBr enlarged the photoresponce of $La_2Ti_2O_7$ to visible light region, thus the composite can be activated to generate more electron and hole pairs. Secondly, the formed BiOBr/$La_2Ti_2O_7$ p-n heterojunction promoted the transfer rate of electrons through the interface and improved the separation efficiency of electron-hole pairs. It is expected that this novel 2D-2D p-n heterostructured photocatalyst would be a promising candidate for environmental remediation.

1. Introduction

Semiconductor photocatalysis, has provided an alternative way as a promising technology for environment purification and solar energy conversion, and has attracted intensive attentions since 1972 [1–4]. Different kinds of semiconductors, such as ZnO [5], CdS [6], WO_3 [7], TiO_2-supported layered compounds [8,9], have been applied as photocatalysts. In recent years, perovskite type semiconductor lanthanide titanate ($La_2Ti_2O_7$) has been served as a new photocatalyst. The report notes that $La_2Ti_2O_7$ with a perovskite-type layered structure is very active. For example, Abe's group synthesized $La_2Ti_2O_7$ which induced water splitting to produce H_2 and O_2 [10,11]. $La_2Ti_2O_7$ showed many good properties such as unique structure with corner-shared TiO_6 octahedrons and La cations[12], low cost, low toxicity, good stability and so on[13–17]. However, $La_2Ti_2O_7$ also possessed some disadvantages such as high recombination rate of photo-produced electron–hole pairs, wide band gap (≈3.8 eV) and poor photocatalytic performance, which limited its practical application. Therefore, it is urgent to develop new strategies to improve the photocatalytic performance and energy efficiency of $La_2Ti_2O_7$. Formation of heterojunction is one of efficient strategies to enhance the separation efficiency of photo-generated charge carries and to promote the transfer rate of electrons. For example, our group synthesized CdS-$Bi_2O_2CO_3$ heterojunction photocatalyst with high activity for the degradation of MO [18]. Wang et al. synthesized Bi_2O_3-Bi_2WO_6 heterojunction photocatalyst with high photocatalytic performance for the degradation of RhB [19]. Lee et al. [20] successfully synthesized TiO_2/CuO composite nanofibers with high activity for H_2 generation. Therefore, it is expected to improve the photocatalytic performance of $La_2Ti_2O_7$ through the combination with other semiconductors to form heterojunctions.

Bismuth oxybromide (BiOBr), owing to the excellent properties and 2D lamellar structure, has aroused strong concern of researchers. Besides, the p-type characteristic of BiOBr endows it to form p-n type heterojunctions when combining with n-type semiconductor. The formed p-n heterojunctions could improve the

* Corresponding authors.
E-mail addresses: andyao@hhu.edu.cn (Y. Ao), pfwang2005@hhu.edu.cn (P. Wang).

http://dx.doi.org/10.1016/j.apcatb.2016.04.050
0926-3373/

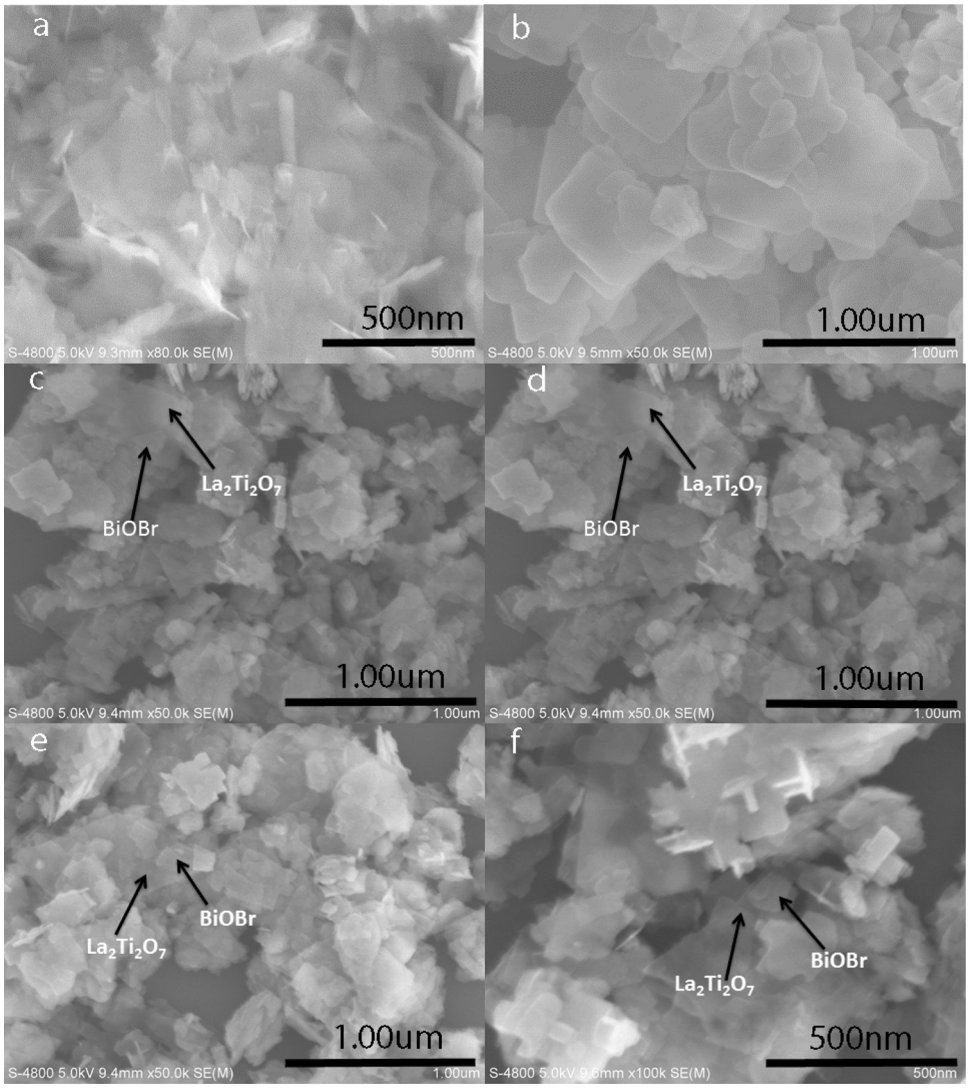

Fig. 1. Typical SEM images of (a) $La_2Ti_2O_7$, (b) BiOBr, (c ~ f) BiOBr/$La_2Ti_2O_7$ composites.

photocatalytic activity efficiently. For example, BiOBr/$BiPO_4$ [21], BiOBr/Bi_2WO_6 [22], were found to be efficient p-n type heterojuntion photocatalysts which exhibit high photocatalytic activity under visible light irradiation. Furthermore, it has proved that BiOBr with narrow band gap (≈2.9 eV) can sensitize wide band gap semiconductor [23]. Therefore, it would be suitable to synthesize p-n type BiOBr/$La_2Ti_2O_7$ heterojunction composites with high photocatalytic performance under visible light irradiation. To the best of our knowledge, the coupling of n-type $La_2Ti_2O_7$ with p-type BiOBr for obtaining of high visible light responsive photocatalytic activity has not been reported previously.

In the present article, we found a facile method for preparation of novel 2D-2D p-n type heterojunction BiOBr/$La_2Ti_2O_7$ nanocomposites. The photocatalytic performance of p-n heterojunction BiOBr/$La_2Ti_2O_7$ composites was investigated by degradation of refractory dye Rhodamine B and phenol under both UV and visible light irradiation. The results indicated that BiOBr/$La_2Ti_2O_7$ could decompose much more contaminates under both UV and visible light irradiation compared to $La_2Ti_2O_7$. Moreover, the phase structure, morphology, optical properties, electrochemical properties of as obtained catalysts were investigated thoroughly. The possible mechanism of enhanced photocatalytic activity for the p-BiOBr/n-$La_2Ti_2O_7$ heterojunction were discussed in detail.

2. Experimental

2.1. Preparation of $La_2Ti_2O_7$

$La_2Ti_2O_7$ nanosheets were synthesized through a hydrothermal method. In a typical process, 20 mmol of lanthanum nitrate hexahydrate was dissolved in 130 ml ultrapure water to form solution A, then 20 mmol of titanium sulfate was added into the solution. Simultaneously, 8 g of sodium hydroxide was dissolved in 20 ml ultrapure water to form solution B. Then, solution B was slowly dripped into the mixture solution under vigorous stirring. Afterwards, the mixture was stirred for another 10 min before it was transferred into a 200 ml of Teflon-lined stainless steel autoclave and heat-treated at 200 °C for 24 h. After cooling, the obtained sample was filtered, and washed by a large amount of ultrapure water. Finally, the sample was dried at 60 °C.

2.2. Preparation of BiOBr/$La_2Ti_2O_7$

A series of BiOBr/$La_2Ti_2O_7$ nanocomposite photocatalysts were prepared by an in-situ growth method. In a typical process, a definite amount of bismuth nitrate pentahydrate and KBr were dissolved in ethylene glycol to form solution A. Simultaneously, 0.3 g $La_2Ti_2O_7$ were added into 80 ml of ultrapure water and ultrasonic

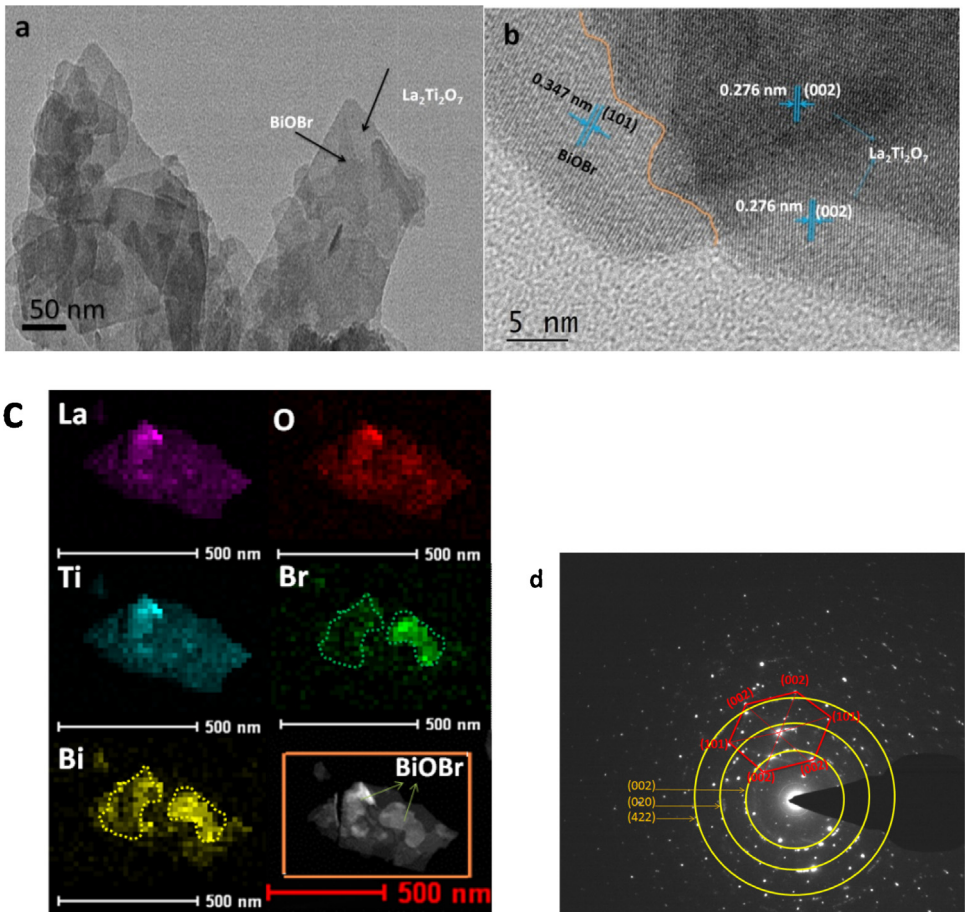

Fig. 2. Typical TEM (a), HRTEM (b), TEM-EDS elemental mapping images (c) and SAED patten (d) of BiOBr/$La_2Ti_2O_7$-3.

for 15 min to disperse and form a uniform suspension B. Then solution A was added slowly into suspension B under vigorous stirring, and continued to stir for 1 h. Next, the mixture were stirred and refluxed in an oil bath at 80 °C for 2 h. After cooling, the products were separated and washed with a large amount of ultrapure water and alcohol. Finally, the samples were dried at 60 °C. The amount of BiOBr was controlled through adjusting the added amounts of bismuth nitrate pentahydrate and KBr. The obtained samples were defined as BiOBr/$La_2Ti_2O_7$-1, BiOBr/$La_2Ti_2O_7$-2, BiOBr/$La_2Ti_2O_7$-3, BiOBr/$La_2Ti_2O_7$-4, for the samples with 9 wt%, 17 wt%, 26 wt% and 43 wt% of BiOBr, respectively. A pure BiOBr control catalyst was also synthesized by the same procedure in the absence of $La_2Ti_2O_7$.

2.3. Characterization

The X-ray diffractometer (XRD, Rigaku, SmartLab) was employed to investigate the phase structure properties of the obtained samples in the range of 2θ between 10° and 80°. The surface morphologies and microstructures of the as-prepared catalysts were obtained by a scanning electron microscope (SEM, Hitachi, S-4800), transmission electron microscopy and high resolution transmission electron microscopy (TEM and HRTEM, JEOL, JEM-2100 (HR)). The element distribution was examined by a SEM equipped with an energy disperse spectroscopy (EDS, TEAM Octane Plus) and TEM-EDS. The UV–vis diffuse reflectance spectra of the as-prepared samples were determined on UV–vis spectrophotometer (Shimadzu, UV3600). BET of the as-prepared samples was investigated to evaluate the absorption property of catalysts. The photocurrent measurements and the electrochemical impedance spectroscopies (EIS) were conducted on an electrochemical station (Chenhua Instruments, CHI660D). Photoluminescence (PL) spectra were recorded on a fluorescence spectrophotometer (Hitachi, F-7000). Trapping experiment and EPR were applied to detect the active species in the photocatalytic reaction.

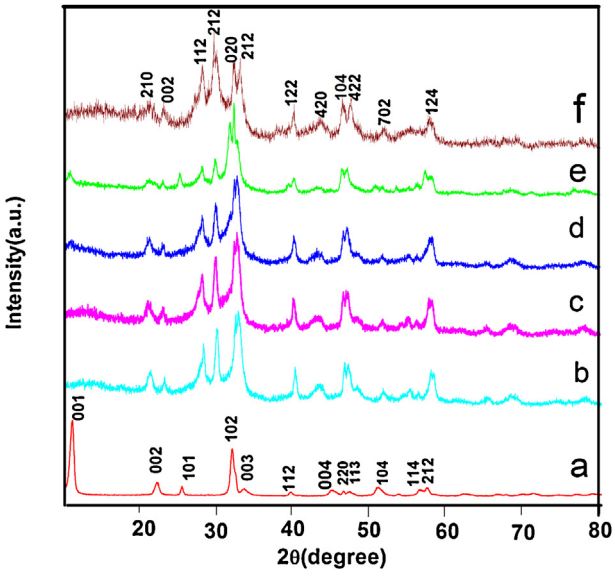

Fig. 3. XRD patterns of (a)BiOBr, (b)BiOBr/$La_2Ti_2O_7$-1 (c)BiOBr/$La_2Ti_2O_7$-2 (d) BiOBr/$La_2Ti_2O_7$-3 (e) BiOBr/$La_2Ti_2O_7$-4 (f) $La_2Ti_2O_7$.

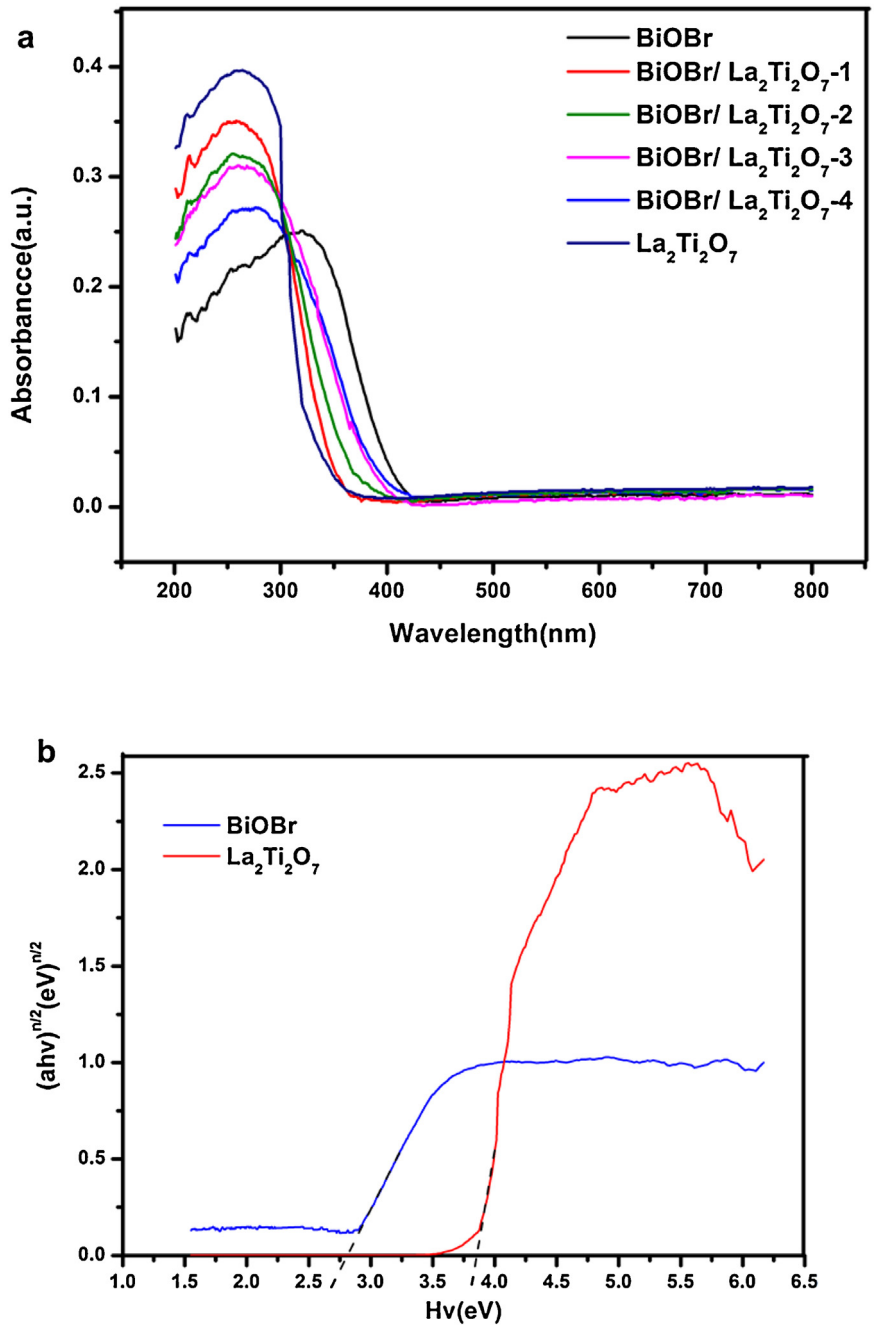

Fig. 4. (a) UV–vis diffuse reflectance spectra for different samples, (b) band gap of pure BiOBr and $La_2Ti_2O_7$.

2.4. Photocatalytic activities

The photocatalytic activity of the as-prepared catalysts was investigated by the photocatalytic degradation of the dye Rhodamine B and phenol under both UV and visible light irradiation. The photocatalytic degradation process of the dye Rhodamine B was carried out as following, 40 mg as-prepared catalysts was added into 100 ml of synthetic Rhodamine B aqueous solution with initial concentration of 10 mg L^{-1}. The light resource was a 300 W xenon lamp (Zhongjiaojinyuan, CEL-HXUV300). Before irradiation, the aqueous suspensions were ultrasonically treated for 2 min and stirred in dark for 90 min. The dark experiments were conducted to achieve adsorption-desorption equilibrium. After the beginning of irradiation, 1.5 ml of suspension was collected at a scheduled interval, then centrifuged and analyzed. The concentration changes of Rhodamine B were assessed by UV–vis spectrophotometer. The degradation process of phenol was same with that of RhB, and the initial concentration of phenol was 5 mg L^{-1}. Moreover, the photocatalytic degradation process of the dye RhB (5 mg L^{-1}) was investigated under visible light irradiation by the same process described above. The light resource was a 300 W Xe lamp with a light filter (400 nm).

3. Results and discussions

3.1. Characterization

The SEM images of the as-prepared samples are showed in Fig. 1. It can be seen clearly from Fig. 1(a) that the morphology of pure $La_2Ti_2O_7$ is composed of nanosheets, and the

size of $La_2Ti_2O_7$ nanosheets is from 0.4 μm to 1 μm. Furthermore, it can be seen that the nanosheets are nearly transparent, which indicates their ultrathin thickness. Fig. 1(b) shows a typical SEM image of BiOBr that consists of smooth and irregular plates, and the size of BiOBr is about 0.3–0.6 μm. Fig. 1(c)–(f) display the morphologies of BiOBr/$La_2Ti_2O_7$-1, BiOBr/$La_2Ti_2O_7$-2, BiOBr/$La_2Ti_2O_7$-3, BiOBr/$La_2Ti_2O_7$-4, respectively. It is found easily that the morphologies of all BiOBr/$La_2Ti_2O_7$ heterojunction composites with various mass ratio of BiOBr are similar. The small 2D BiOBr nanoplates are dispersed on the large 2D $La_2Ti_2O_7$ thin nanosheets. In addition, we can obtain that the size of BiOBr in BiOBr/$La_2Ti_2O_7$ nanocomposites is obvious smaller than that of pure BiOBr. It may be attributed to the fact that the growth of BiOBr nanoplates is greatly inhibited by $La_2Ti_2O_7$. Similar observation has been reported in previous literature [24].

The TEM and HRTEM were used to further investigate the morphology and microstructure of the obtained photocatalyst. Fig. 2(a, b) shows typical TEM and HRTEM images of BiOBr/$La_2Ti_2O_7$-3 composite with the best mass ratio of BiOBr. It can be seen clearly in Fig. 2(a) that small 2D BiOBr nanoplates disperse on the surface of larger 2D $La_2Ti_2O_7$ thin nanosheets. It is in good agreement with the SEM results. Besides, the fringes with lattice spacing of $La_2Ti_2O_7$ and BiOBr are observed easily (as shown in Fig. 2(b)). The lattice spacing are 0.276 nm and 0.347 nm, which is in accordance with (002) $La_2Ti_2O_7$[25] and (101) BiOBr [26], respectively. Furthermore, it can be seen that there is a clear interface of the two different phase of $La_2Ti_2O_7$ and (101) BiOBr (marked by a orange line). The results demonstrate the formation of BiOBr/$La_2Ti_2O_7$ heterojunction [27,28]. In addition, it is found that the 2D-2D *p-n* type BiOBr/$La_2Ti_2O_7$ heterojunctions are formed with large and tight contact interface. Therefore, it is expected that the formed heterojunction is advantageous for the separation of the photogenerated charge carriers[29–31]. The TEM-EDS mapping images, which are shown in Fig. 2(c), prove the presence of La, Ti, Bi, Br, and O elements in the BiOBr/$La_2Ti_2O_7$ composites. It can also be seen that the BiOBr (represented by Bi and Br elements) nanoplates are deposited on the surface of nanosheets $La_2Ti_2O_7$. Furthermore, the boundaries between BiOBr and $La_2Ti_2O_7$ can be seen clearly from the mapping images. All these results further indicated the formation of heterojunctions between BiOBr and $La_2Ti_2O_7$. The selected area electron diffraction (SAED) pattern of the BiOBr/$La_2Ti_2O_7$ composite is represented in Fig. 2(d). The SAED pattern of the composite shows the coexistence of the tetragonal phase of BiOBr and the monoclinic of $La_2Ti_2O_7$. It coincides well with the XRD pattern of the BiOBr/$La_2Ti_2O_7$ heterojunction composites which will be shown in the following section. The brighter rings represented by yellow color correspond to the (002), (020) and (422) planes of the monoclinic of $La_2Ti_2O_7$, respectively. While the light spots represented by red color correspond to the (101) and (002) planes of the tetragonal phase of BiOBr, respectively. The SAED pattern of the BiOBr/$La_2Ti_2O_7$ heterojunction composite confirms that the product is well crystallized.

The crystal structure and phase composition of the as obtained catalysts are measured by powder X-ray diffraction pattern (PXRD), the obtained results are displayed in Fig. 3. As shown in Fig. 3(a, f), the characteristic diffraction peaks of pure $La_2Ti_2O_7$ and BiOBr are in good agreement with the monoclinic $La_2Ti_2O_7$ (JCPDS card 28-0517) [32] and the tetragonal phase of BiOBr (JCPDS 73-2061) [33], respectively. Besides, it can be also seen that all diffraction peaks of BiOBr/$La_2Ti_2O_7$ composites are in conformity with diffraction peaks of BiOBr and $La_2Ti_2O_7$. Any impurity peaks cannot be discovered in all diffraction peaks of BiOBr/$La_2Ti_2O_7$ composites. It indicates the high purity of the obtained BiOBr/$La_2Ti_2O_7$ composites [34]. In addition, all peak intensity of BiOBr becomes strong along with the increasing content of BiOBr in BiOBr/$La_2Ti_2O_7$ composites. While the peak intensity of $La_2Ti_2O_7$ becomes weaker as

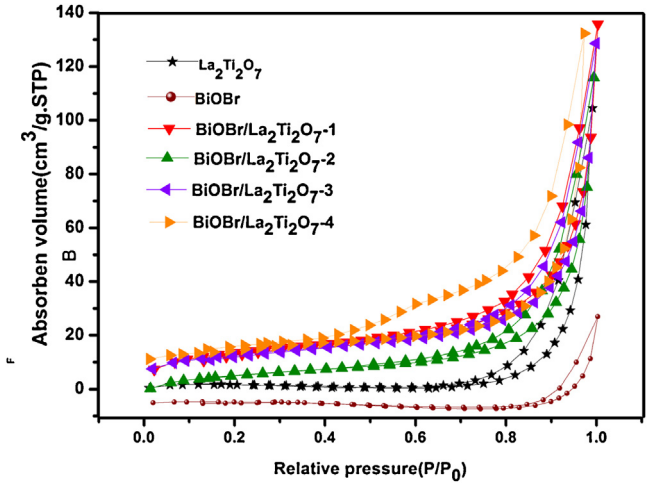

Fig. 5. Nitrogen adsorption-desorption isotherms of as-prepared samples.

the content of BiOBr increases. It indicates that more BiOBr are deposited onto the surface of $La_2Ti_2O_7$ as its content increases.

The optical properties of the different samples were investigated by UV–vis diffuse reflectance spectrum (DRS), and the obtained results are displayed in Fig. 4(a). Obviously, pure $La_2Ti_2O_7$ merely responds to the ultraviolet light and its optical absorption edge lies at about 352 nm. While pure BiOBr can respond to the visible light and its optical absorption edge locates at about 430 nm. Besides, we can find that the optical absorption edge of BiOBr/$La_2Ti_2O_7$ composites exhibit red shift along with the increased mass ratio of BiOBr. It illustrates that the decorated of BiOBr enhance the photoresponse of $La_2Ti_2O_7$ in visible range. The results indicate that BiOBr/$La_2Ti_2O_7$ composites can be excited thus generate more charge carries under visible light irradiation. The band gap (Eg) of semiconductors can be determined from DRS plots, which follow the formula [35]: $ahv = A(hv-Eg)^{n/2}$. Where a, h, m, Eg and A are absorption coefficient, Planck constant, light frequency, band gap energy, and a constant, respectively. Among them, n is determined by the type of optical transition of a semiconductor (n = 1 for direct transition and n = 4 for indirect transition). As previous literatures reported, the n value of $La_2Ti_2O_7$ was 1[36] while the n value of BiOBr was 4 [27]. From the plot of $(ahv)^2$ versus (hv) in Fig. 4(b), the Eg of $La_2Ti_2O_7$ and BiOBr are estimated to be 3.72 and 2.78 eV, respectively. Based on above results, it can be concluded that the synergistic effect of the formed 2D-2D *p-n* type heterojunction and the effective utilization of the incident light would endow BiOBr/$La_2Ti_2O_7$ composites with high photocatalytic activity.

Fig. 5 shows the nitrogen adsorption-desorption isotherms of as-prepared samples. According to the Brunauer-Deming-Deming-Teller (BDDT) classification, the majority of physisorption isotherms can be classified into six types. Clearly, all the as-prepared samples exhibit a type-IV nitrogen isotherms, demonstrating the presence of mesopores [37]. Besides, the hysteresis loops of the isotherms can be found easily, and it is categorized as type H3, indicating the presence of slit-shaped pores [38]. The slit-shaped pores formed among the aggregation of plates-like particles [39]. This result is consistent with the SEM and TEM images. It can be expected that excessive BiOBr tends to aggregate along with the increased contents of BiOBr. The BET surface area (A_{BET}) values of all the samples were calculated to be 32.6, 6.8, 49.7, 40.1, 44.5, 40.0 m^2/g for pure $La_2Ti_2O_7$, BiOBr, BiOBr/$La_2Ti_2O_7$-1, BiOBr/$La_2Ti_2O_7$-2, BiOBr/$La_2Ti_2O_7$-3 and BiOBr/$La_2Ti_2O_7$-4, respectively. The BET values of composites are larger than pure $La_2Ti_2O_7$ and BiOBr. However, the adsorption results show that the adsorption percent of RhB is not proportional with the surface area.

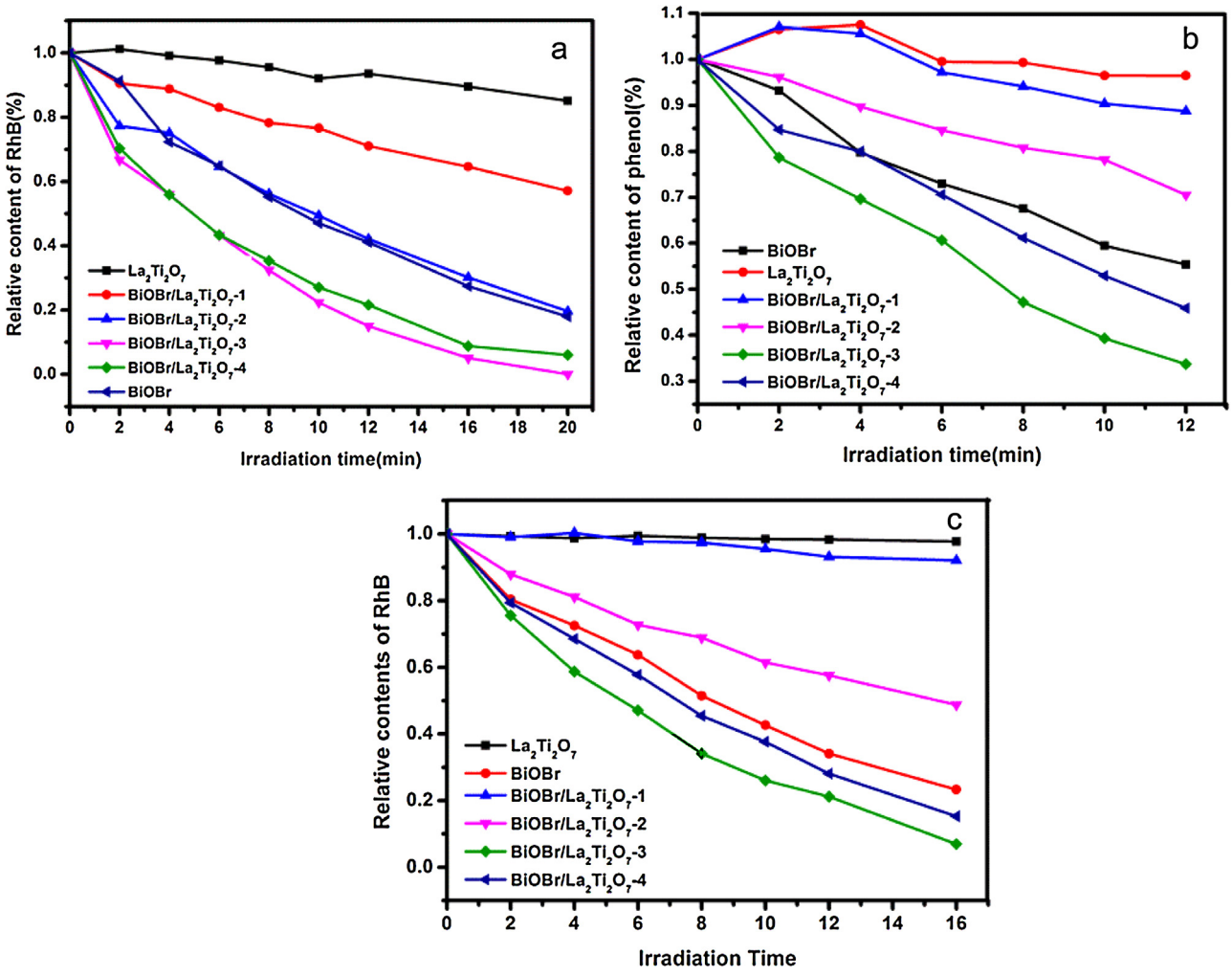

Fig. 6. Photocatalytic degradation of (a) phenol (initial concentration of 5 mg/L), (b) RhB (initial concentration of 10 mg/L) in the presence of as-prepared samples under UV light irradiation, (c) Photocatalytic degradation of RhB (initial concentration of 5 mg/L) in the presence of as-prepared samples under visible light irradiation.

The adsorption percents are 6.1%, 54.3%, 8.1%, 11.8%, 20.8% and 35.4% for $La_2Ti_2O_7$, BiOBr, BiOBr/$La_2Ti_2O_7$-1, BiOBr/$La_2Ti_2O_7$-2, BiOBr/$La_2Ti_2O_7$-3 and BiOBr/$La_2Ti_2O_7$-4, respectively. It is proportional with the content of BiOBr in the composite.

3.2. Photocatalytic activity

The photocatalytic performance of the as-prepared samples was investigated by the degradation of model polluted dye RhodamineB (RhB) and phenol under both UV and visible light irradiation. The photocatalytic degradation percent of phenol and RhB are very low and can be ignored without adding any photocatalysts [40]. Fig. 6 displays the photocatalytic degradation of RhB and phenol in the presence of different samples under UV and visible light irradiation. As presented in Fig. 6(a), it is easy to obtain that the photocatalytic degradation percent of RhB by BiOBr/$La_2Ti_2O_7$ composites increases along with the increasing contents of BiOBr firstly, and then decreases when the mass ratio of BiOBr exceeds 26 wt%. BiOBr/$La_2Ti_2O_7$-3 composite exhibits the best photocatalytic performance in the as-prepared samples. The results are attributed to the following two reasons: (1) in a certain range, the increased contents of BiOBr lead to the formation of more heterojunction in BiOBr/$La_2Ti_2O_7$ composites. The *p-n* type heterojunctions can improve the separation efficiency of photogenerated charge carries and enhance the transfer of electrons in the interfacial domain, thus BiOBr/$La_2Ti_2O_7$ composites exhibit higher photocatalytic activity. (2) When the mass ratio of BiOBr exceeds 26 wt%, redundant BiOBr is easy to aggregate. Therefore, the aggregated BiOBr cannot contact with $La_2Ti_2O_7$ to form efficient heterojunctions.

The above results reveal that the as-prepared catalysts can decompose dye RhB efficiently, the degradation of non-dye compound is also investigated. Fig. 6(b) shows the photocatalytic degradation of phenol under UV light irradiation. As shown in Fig. 6(b), the degradation percent of phenol by all samples follow the order: BiOBr/$La_2Ti_2O_7$-3 > BiOBr/$La_2Ti_2O_7$-4 > BiOBr > BiOBr/$La_2Ti_2O_7$-2 > BiOBr/$La_2Ti_2O_7$-1 > $La_2Ti_2O_7$. It is in accordance with the result of RhB degradation under UV light irradiation. BiOBr/$La_2Ti_2O_7$-3 composite exhibits the highest photocatalytic activity on the degradation of both RhB and phenol under UV light irradiation.

In addition, we also investigated the photocatalytic performance of the obtained catalysts under visible light irradiation. The results are shown in Fig. 6(c). It can be seen obviously that the obtained samples can degrade RhB efficiently under visible light. The trend of degradation percent of RhB is consistent with that under UV light irradiation. In addition, BiOBr/$La_2Ti_2O_7$-3 exhibits the highest activity, which is in good agreement with the results of phenol and RhB degradation under UV light. All in all, the as-prepared composite photocatalysts exhibit higher photocatalytic performance than pure $La_2Ti_2O_7$ in the photocatalytic degradation of phenol and RhB under both UV and visible light irradiation.

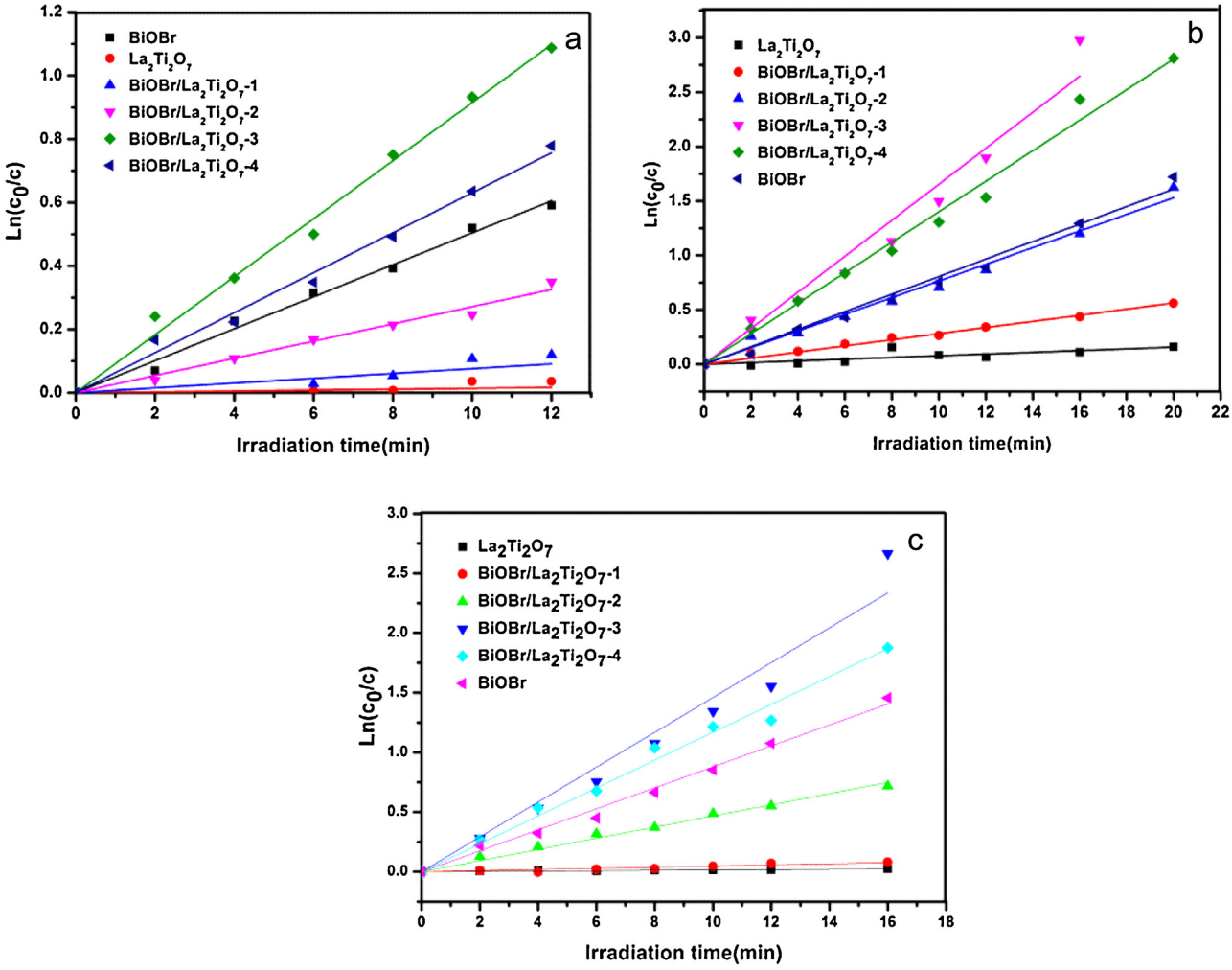

Fig. 7. Linear transform $\ln(c_0/c) = k_{app}t$ of the kinetic curves for phenol and RhB degradation by different samples.

In addition, to have a better understanding of the reaction kinetics for phenol and RhB degradation, the experimental data are fitted by a pseudo-first-order kinetic model [41]. Fig. 7 shows the pseudo-first-order kinetics data for the photocatalytic degradation of phenol and RhB by different photocatalysts. All fitting curves of the irradiation time (t) against $\ln(C_0/C)$ are nearly linear and the correlation coefficients obtained are more than 0.98. Therefore, the reaction kinetics of the phenol and RhB degradation could be described properly by a pseudo-first-order kinetic model [42]. Fig. 7(a) displays the reaction kinetics of phenol under UV light irradiation. The corresponding rate constants were calculated to be 0.0014 min^{-1}, 0.0076 min^{-1}, 0.027 min^{-1}, 0.050 min^{-1}, 0.063 min^{-1}, 0.092 min^{-1} for pure $La_2Ti_2O_7$, BiOBr/$La_2Ti_2O_7$-1, BiOBr/$La_2Ti_2O_7$-2, pure BiOBr, BiOBr/$La_2Ti_2O_7$-4, BiOBr/$La_2Ti_2O_7$-3, respectively. BiOBr/$La_2Ti_2O_7$-3 composite exhibits the highest k values (0.092 min^{-1}), which is about 66 times higher than that of $La_2Ti_2O_7$ and 2 times higher than that of BiOBr. In addition, the corresponding rate constant of the as-prepared samples for the degradation of RhB under UV light irradiation are also calculated to be 0.17 min^{-1}, 0.14 min^{-1}, 0.081 min^{-1}, 0.077 min^{-1}, 0.028 min^{-1}, 0.0079 min^{-1} for BiOBr/$La_2Ti_2O_7$-3, BiOBr/$La_2Ti_2O_7$-4, pure BiOBr, BiOBr/$La_2Ti_2O_7$-2, BiOBr/$La_2Ti_2O_7$-1, pure $La_2Ti_2O_7$, respectively. (as shown in Fig. 7(b)). It can be found that the highest k values (0.17 min^{-1}) of BiOBr/$La_2Ti_2O_7$-3 composite is about 21 times higher than that of $La_2Ti_2O_7$ and 2 times higher than that of BiOBr. Furthermore, for the decomposition of RhB under visible light irradiation (as shown in Fig. 7(c)), the corresponding rate constant are calculated to be 0.15 min^{-1}, 0.12 min^{-1}, 0.088 min^{-1}, 0.047 min^{-1}, 0.0048 min^{-1}, 0.0015 min^{-1} for BiOBr/$La_2Ti_2O_7$-3, BiOBr/$La_2Ti_2O_7$-4, pure BiOBr, BiOBr/$La_2Ti_2O_7$-2, BiOBr/$La_2Ti_2O_7$-1, pure $La_2Ti_2O_7$, respectively. The highest k values (0.15 min^{-1}) of BiOBr/$La_2Ti_2O_7$-3 composite is about 99 times higher than that of $La_2Ti_2O_7$ and 2 times higher than that of BiOBr. All these results illustrate that the coupling of $La_2Ti_2O_7$ with BiOBr can improve the photocatalytic performance of $La_2Ti_2O_7$ efficiently under both UV and visible light irradiation.

3.3. *Mechanism of the enhanced photocatalytic activity for BiOBr/$La_2Ti_2O_7$ heterostructure*

The trapping experiment was conducted to determine what kind of radicals play a main role in the degradation of RhB. In this reaction system, tert-butanol (5 mmol L^{-1}), p-benzoquinone (1 mmol L^{-1}) and EDTA-Na_2 (5 mmol L^{-1}) were chosen as the scavengers of $^{\bullet}OH$, $^{\bullet}O_2^-$ radicals and holes, respectively [43,44]. Fig. 8 displays the degradation of RhB by BiOBr/$La_2Ti_2O_7$-3 with the addition of tert-butanol, p-benzoquinone and EDTA-Na_2. Obviously, when tert-butanol was added, the degradation of dye RhB has no apparent change compared to the condition with no scavenger. It indicates that $^{\bullet}OH$ radicals play a little role in the photocatalytic degradation of RhB. However, the photocatalytic degradation percent of RhB decreases to nearly zero when EDTA-Na_2 was added. It

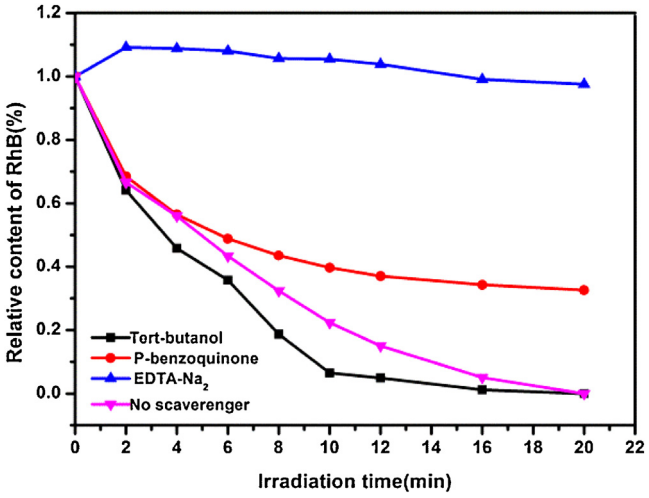

Fig. 8. Effect of scavengers on the photocatalytic degradation of RhB by BiOBr/$La_2Ti_2O_7$-3 under UV light irradiation.

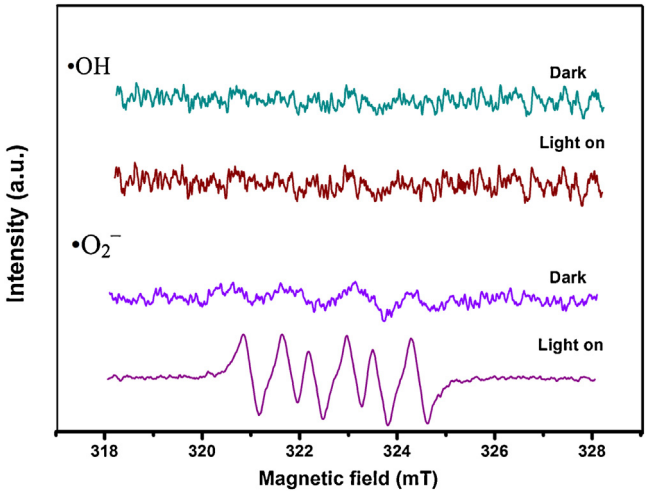

Fig. 9. EPR test of BiOBr/$La_2Ti_2O_7$-3 under visible irradiation.

indicates that holes are served as the main radicals to participate in the photocatalytic degradation of RhB. Besides, the degradation of RhB is depressed when p-benzoquinone was added, which reveals that $^{\bullet}O_2^-$ radicals also take part in the photocatalytic degradation of RhB. Therefore, it can be concluded that the CB electrons can react with oxygen molecule to form $^{\bullet}O_2^-$ radicals, then $^{\bullet}O_2^-$ radicals and holes participate in the degradation reaction of RhB adsorbed on the surface of photocatalysts. EPR spectra were also used to detect the active species in the photocatalytic reaction [45,46]. DMPO was chosen as a scavenger agent for the active species. As shown in Fig. 9, six characteristic peaks of the DMPO—O_2^- adducts can be observed for BiOBr/$La_2Ti_2O_7$-3 composites under visible light irradiation [47]. But, the four characteristic peaks of DMPO—OH adducts (1:2:2:1 quartet pattern) are not observed in BiOBr/$La_2Ti_2O_7$-3 composites under visible light irradiation [48]. From Fig. 9, it can be seen clearly that no EPR signals are observed when the reaction was performed in the dark, while the signals corresponding to the characteristic peaks of DMPO—O_2^- adducts are observed under visible light irradiation. Thus $^{\bullet}O_2^-$ radicals take apart in the decomposition of pollutant, which is in good agreement with the results of trapping experiment. In addition, EPR signals represented of the characteristic peaks of DMPO—OH adducts were not observed when the reaction was performed under visible light irradiation. It indicates that photo-generated holes on the surface of BiOBr are not expected to react with OH^-/H_2O to form •OH, suggesting that the decomposition of rhodamine B could be attributed to a direct reaction with the photogenerated holes or with superoxide radicals. The trapping experiments and EPR results indicate that holes (served as the main radicals) and $^{\bullet}O_2^-$ radicals both take part in the degradation of the pollutant absorbed on the surface of photocatalysts.

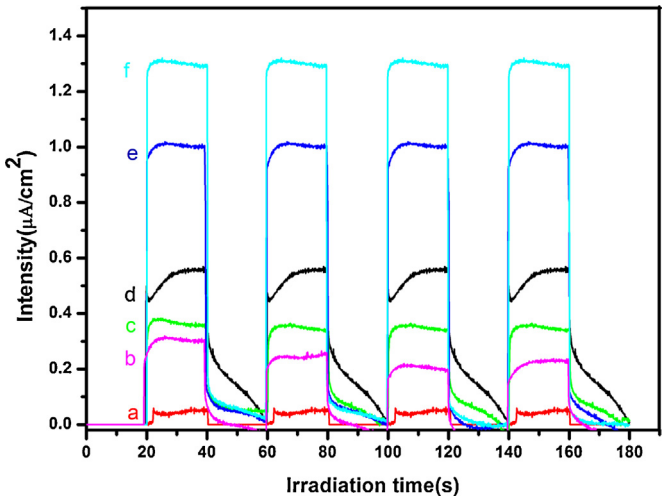

Fig. 10. Photocurrent responses of the as-prepared samples.

It is well known that the photocatalytic activity is closely related to the transfer rate of photo-generated charge pairs. The photocurrent responses of as-prepared samples were measured on a CHI660D electrochemical workstation (Shanghai, Chenhua, China) via a standard three-electrode system. In this system, BiOBr/$La_2Ti_2O_7$ films, platinum wire and Ag/AgCl were served as working electrode, counter electrode and reference electrode, respectively [49]. The source of the visible light is a 250 W metal halide (Instrumental Corporation of Beijing Normal University) with a light filter. Besides, the electrolyte was 0.1 M Na_2SO_4. Through switching on or off of the lamp during the identical interval time, the photocurrent responds of samples were recorded, and the obtained results are displayed in Fig. 10. Obviously, we can achieve a fast and uniform photocurrent response in all electrodes. It can be seen clearly that the photocurrent density first increases then decreases along with the increasing contents of BiOBr in the BiOBr/$La_2Ti_2O_7$ composites. The trend of photocurrent is consistent with the result of photocatalytic activity. Thus it is concluded that the formed 2D-2D *p-n* type heterojunctions can efficiently promote the transfer of electrons in the interface. In addition, the photocurrent intensity of BiOBr/$La_2Ti_2O_7$-3 composite is much higher than BiOBr and $La_2Ti_2O_7$, which reveals that BiOBr/$La_2Ti_2O_7$-3 composite has the longest lifetime of photogenerated charge carrier [50,51]. It is also in good agreement with the highest photocatalytic activity. Therefore, it is concluded that the high transfer rate of electrons also contributes to the high photocatalytic performance.

In order to furtherly estimate the charge-carriers migration, the electrochemical impedance spectroscopies (EIS) were recorded [52]. The EIS was measured at open circuit potential under the same condition with photocurrent experiment. The amplitude of the sinusoidal wave was 10 mV, and its frequency ranged from 100 kHz to 0.05 Hz. Fig. 11 shows the EIS of all samples. The typical EIS are presented as Nyquist plots. It is seen clearly from Fig. 11 that the size of the semicircle of BiOBr/$La_2Ti_2O_7$-3 composite in the plot is the smallest in all samples. It indicates that electrons migration speed of BiOBr/$La_2Ti_2O_7$-3 composite is more rapid than others. The result is in consistent with that of photocurrent.

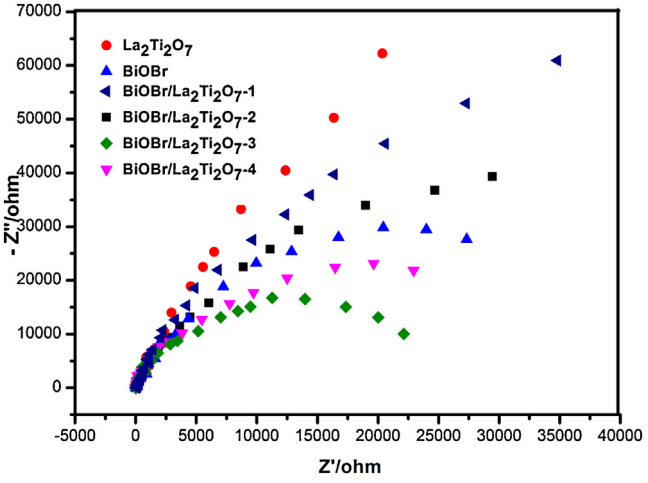

Fig. 11. EIS property of $La_2Ti_2O_7$, BiOBr, BiOBr/$La_2Ti_2O_7$ composites.

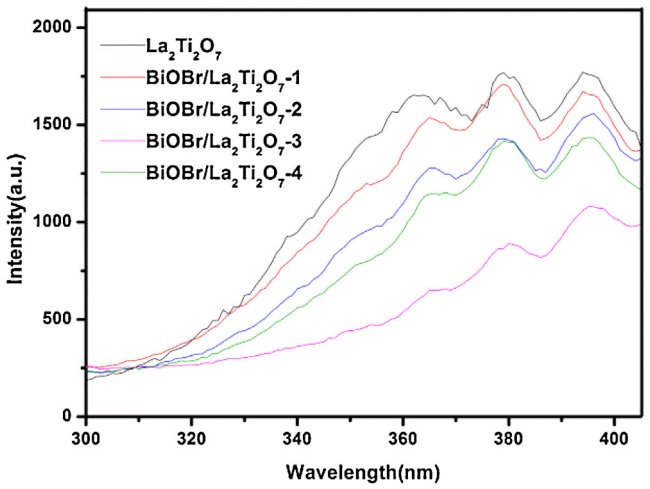

Fig. 13. Photoluminescence spectra of $La_2Ti_2O_7$, BiOBr/$La_2Ti_2O_7$ composites.

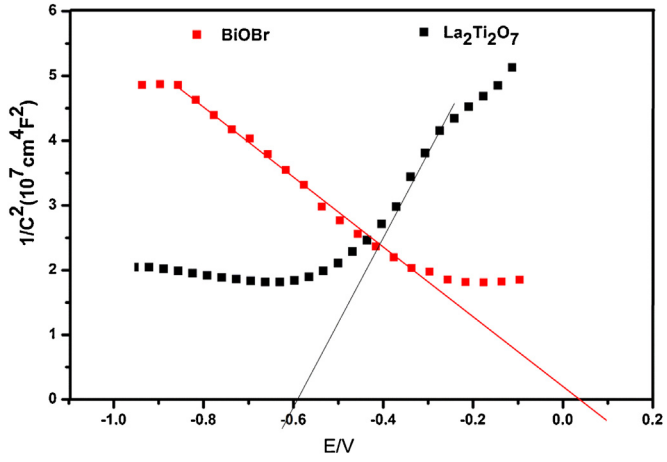

Fig. 12. Mott-Schottky plots of pure $La_2Ti_2O_7$ and BiOBr.

Mott-Schottky analysis was obtained by conducting an impedance-potential spectroscopy on a CHI660D electrochemical workstation (Shanghai Chenhua, China). In the process, the frequency was 1000 Hz, the electrolyte was 0.1 M Na_2SO_4, and the potential ranged from −1 V to 0 V. Mott-Schottky relationships are expressed as C^{-2} vs. potential, where C is the space charge capacitance of the semiconductor electrode. The slopes and X-intercepts of such plots are often used to judge the n- or p-type of semiconductors and estimate their flat-band potential (E_{fb}) [53]. Fig. 12 shows the Mott-Schottky plot of the as-prepared BiOBr, $La_2Ti_2O_7$, respectively. It can be seen clearly that the slope of BiOBr is negative, while $La_2Ti_2O_7$ exhibits a positive slope in the linear region of the plot. It implies that BiOBr exhibits p-type semiconductor character, and $La_2Ti_2O_7$ exhibits n-type semiconductor character [54]. Furthermore, the flat-band potentials of BiOBr and $La_2Ti_2O_7$ are calculated to be 0.05 and −0.59 V vs. Ag/AgCl (0.25 and −0.39 V vs NHE) [55], respectively.

As we all known, the photocatalytic activity is not just related with the electrons transfer rate, the recombination rate of photo-generated charge carries was inseparable with the photocatalytic activity. The separation efficiency of electron-hole pairs was assessed by photoluminescence (PL) spectra, and higher intensity reveals a increased recombination rate of photo-generated charge carries [56]. Fig. 13 shows the PL spectra of different samples. It is easy to found that the emission peaks appear at about 396 nm. Besides, the photoluminescence intensity of the all BiOBr/$La_2Ti_2O_7$ composites is lower than that of pure $La_2Ti_2O_7$. It indicates that BiOBr/$La_2Ti_2O_7$ composites exhibit higher separation rate of photo-generated charge pairs than pure $La_2Ti_2O_7$. The result is in good agreement with the photocurrent and EIS results. In addition, the PL intensity of BiOBr/$La_2Ti_2O_7$-3 composite is the lowest among all samples. The result indicates that it exhibits lower recombination rate of electron-hole pairs than others, which contributes to the highest photocatalytic activity. The above results are attributed to the formation of p-n type heterojunctions between BiOBr and $La_2Ti_2O_7$ in the composites. The formed p-n heterojunctions can enhance the separation efficiency of charge carries [57]. Therefore, the higher transfer rate of electrons and separation efficiency of electron-hole pairs urge more holes directly react with the pollutants adsorbed on the surface of photocatalysts, thus boost the photocatalytic performance.

The generation, separation, and transfer of charge carries, which are closely related with photocatalytic activity, are investigated as above mentioned. In order to further illustrate that the high photocatalytic activity is due to the formation of BiOBr/$La_2Ti_2O_7$ heterojunctions, the physical mixing sample of $La_2Ti_2O_7$ and BiOBr was investigated. In the experiment, the contents of BiOBr in physical mixture was same with that of BiOBr/$La_2Ti_2O_7$-3 composite. 40 mg mixture was added into 100 mL of the dye RhB solution with the initial concentration of 10 mg L^{-1}, and the experiment conditions were same with that of BiOBr/$La_2Ti_2O_7$-3 composite. Fig. 14 shows the degradation of RhB by pure $La_2Ti_2O_7$, BiOBr, BiOBr/$La_2Ti_2O_7$-3, and physical mixture. It can be seen clearly that the decomposition percent of these samples follow the following order: BiOBr/$La_2Ti_2O_7$-3 > BiOBr > physical mixture > $La_2Ti_2O_7$. The result is ascribed to the following reasons: (1) Due to the existence of BiOBr, the physical mixture exhibits higher photocatalytic degradation percent of RhB than pure $La_2Ti_2O_7$. (2) The formed 2D-2D p-n type heterojunctions act as the main factor, which contributes to the higher photocatalytic activity of BiOBr/$La_2Ti_2O_7$-3 composite than the physical mixture. The results further indicate that the heterojunctions between BiOBr and $La_2Ti_2O_7$ are formed thus enhance the photocatalytic performance.

Based on the above results and discussions, we believe that p–n heterojunction formed in the p-BiOBr/n-$La_2Ti_2O_7$ composites played a dominating role in the efficient separation of photoinduced electron–hole pairs. In order to clearly understand the formation of p-BiOBr/n-$La_2Ti_2O_7$ heterojunction, the band positions of BiOBr and $La_2Ti_2O_7$ were investigated. As mentioned above, the band gap of BiOBr and $La_2Ti_2O_7$ is 2.78 eV and 3.72 eV, respectively. The band positions of BiOBr and $La_2Ti_2O_7$ were calcu-

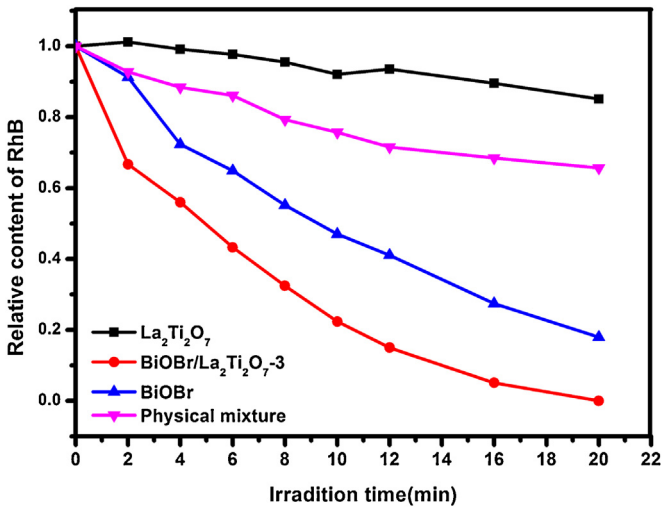

Fig. 14. Comparison of the photocatalytic activity of different samples for RhB degradation.

lated by the following empirical formulas [58]: $E_{VB} = X_{photocatalyst} - E^e + 0.5Eg$. Where E_{VB} is the valence band (VB) potentials, X is the electronegativity of the semiconductor (which is the geometric mean of the electronegativity of the constituent atoms), E^e is the energy of free electrons on the hydrogen scale (4.5 eV). Herein, the E_{VB} of BiOBr and $La_2Ti_2O_7$ were calculated to be 3.1 eV and 3.26 eV, respectively. According to the $E_{CB} = E_{VB} - Eg$, the E_{CB} of BiOBr and $La_2Ti_2O_7$ were calculated to be 0.22 eV and −0.39 eV, respectively. However, it is important to note that this equation is empirical, theoretical, and only takes electronegativity into account [59]. Thus, E_{CB} calculated through this equation just has a relative value. To further elucidate the band positions of BiOBr and $La_2Ti_2O_7$, electrochemical flat-band potential measurements were carried out, as shown in Fig. 12. As we all known, the flat-band potential is slightly lower than CB potential. Therefore, it is believed that the CB potential (E_{CB}) is very close to the V_{fb} [46], and E_{CB} equal to V_{fb} approximately. Besides, the VB potential (E_{VB}) was calculated according to equation $E_{VB} = Eg + E_{CB}$. As mentioned above, the E_{CB} of BiOBr and $La_2Ti_2O_7$ are considered to be about 0.25 and −0.39 eV, respectively. Therefore, the E_{VB} of BiOBr and $La_2Ti_2O_7$ are calculated to be 3.03 eV and 3.33 eV, respectively. The results are displayed in Fig. 15(a). The band position suggests that the band structure of pure $La_2Ti_2O_7$ and BiOBr is nested before contact, the Fermi levels of p-type BiOBr is near below, while the Fermi levels of n-type $La_2Ti_2O_7$ is near above, which seems to be hard to conduct the photocatalytic reaction. However, according to the general p-n junction formation process reported in literatures [51,60]. The whole energy band of BiOBr moved up whereas that of $La_2Ti_2O_7$ shift down until an equilibrium state of Fermi levels (EF) of BiOBr and $La_2Ti_2O_7$ was obtained after contact.

As shown in Fig. 15(b), the CB of BiOBr is higher than that of $La_2Ti_2O_7$, while the VB of BiOBr is lower than that of $La_2Ti_2O_7$ after contact. Thus, under UV light irradiation, both BiOBr and $La_2Ti_2O_7$ can be activated to generate electron-hole pairs. Firstly, the electrons excited in the VB of BiOBr and $La_2Ti_2O_7$ then transfer to the CB of BiOBr and $La_2Ti_2O_7$, respectively. The holes remain in the VB of BiOBr and $La_2Ti_2O_7$, respectively. Secondly, the electrons in the CB of BiOBr can migrate to the CB of $La_2Ti_2O_7$ due to the higher CB of BiOBr. The transferred electrons are further trapped by molecular oxygen to form $^{\bullet}O_2^-$ radicals. While the holes on the VB of $La_2Ti_2O_7$ transfer to the VB of BiOBr because of the higher VB of $La_2Ti_2O_7$. Finally, the $^{\bullet}O_2^-$ radicals and holes both participate in the photocatalytic degradation reaction of pollutants adsorbed on the surface of photocatalysts. Under visible light irradiation, only BiOBr can be activated to generate electron-hole pairs. Then the photo-

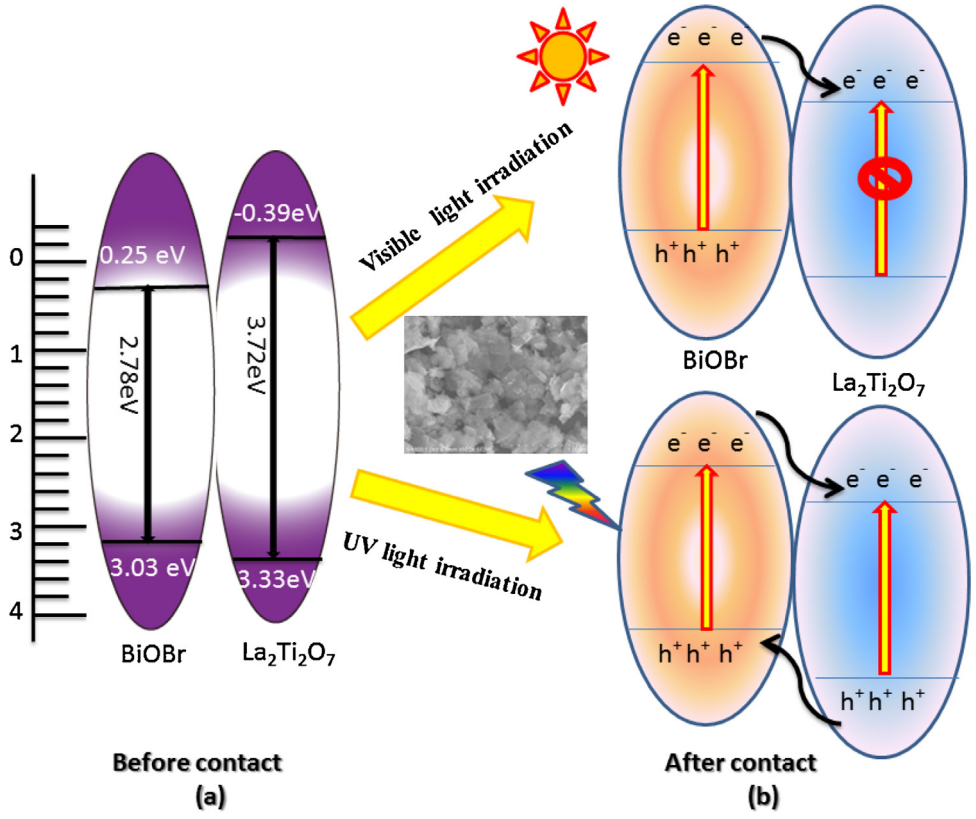

Fig. 15. Schematic diagram of the possible photocatalytic mechanism over BiOBr/$La_2Ti_2O_7$ under both UV and visible light irradiation.

generated electrons can also be transferred to the CB of $La_2Ti_2O_7$ through the formed *p-n* heterojunctions. The transferred electrons are further trapped by molecular oxygen to form $^{\bullet}O_2^-$ radicals. The $^{\bullet}O_2^-$ radicals can induce the degradation of pollutants. Furthermore, the photo-generated holes in the VB of BiOBr can migrate to the surface of the photocatalyst and degrade the adsorbed pollutants directly. All in all, the formed *p-n* type heterojunctions in the BiOBr/$La_2Ti_2O_7$ composites not only accelerates the transition rate of electrons in the junctions interface, but also restrains the recombination of the photogenerated electron-hole pairs. Therefore, the coupling of $La_2Ti_2O_7$ with BiOBr can induce enhanced photocatalytic activity under both UV and visible light irradiation.

4. Conclusions

In summary, novel 2D-2D *p-n* type BiOBr/$La_2Ti_2O_7$ heterojunction photocatalysts were successfully fabricated via a simple method. The photocatalytic performance of the as-prepared BiOBr/$La_2Ti_2O_7$ composites first increased then decreased along with the increasing contents of BiOBr, and BiOBr/$La_2Ti_2O_7$-3 (26 wt%) composite exhibited the highest photocatalytic activity for the degradation of RhB and phenol under both UV and visible light irradiation. DRS results illustrated that BiOBr acted as a sensitizer to enhance the photoresponce of $La_2Ti_2O_7$ in the visible range, thus lead to the generation of more electron-hole pairs under visible light irradiation. In addition, the heterojunction formed between BiOBr and $La_2Ti_2O_7$ can facilitate to enhance the separation efficiency of photogenerated charge carries and improve the transfer rate of electrons in the interface, which were confirmed by PL, photocurrent and EIS. The formation of *p-n* heterojunction was the main factor, which contribute to the enhancement of photocatalytic performance for $La_2Ti_2O_7$ under both UV and visible light irradiation.

Acknowledgements

We are grateful for grants from National Science Funds for Creative Research Groups of China (No.51421006), Program for Changjiang Scholars and Innovative Research Team in University (No. IRT13061), National Science Fund for Distinguished Young Scholars (No. 51225901), the National Science Fundation of China for Excellent Young Scholars (No. 51422902), the Key Program of National Natural Science Foundation of China (No. 41430751), the National Natural Science Foundation of China (No. 51579073), Natural Science Foundation of Jiangsu Province (BK20141417), and PAPD.

References

[1] P. Liu, J. Nisar, B.S. Sa, B. Pathak, R. Ahuja, Anion–anion mediated coupling in layered perovskite $La_2Ti_2O_7$ for visible light photocatalysis, J. Phys. Chem. C 117 (27) (2013) 13845–13852.
[2] Y. Li, J.F. Niu, E.X. Shang, C. John, Photochemical transformation and photoinduced toxicity reduction of silver nanoparticles in the presence of perfluorocarboxylic acids under UV irradiation, Environ. Sci. Technol. 48 (9) (2014) 4946–4953.
[3] Y. Li, J.F. Niu, E.X. Shang, C. John Charles, Synergistic photogeneration of reactive oxygen species by dissolved organic matter and C_{60} in aqueous phase, Environ. Sci. Technol. 49 (2) (2015) 965–973.
[4] A. Kudo, Y. Miseki, Heterogeneous photocatalyst materials for water splitting, Chem. Soc. Rev. 38 (1) (2009) 253–278.
[5] R. Lamba, A. Umar, S.K. Mehta, S.K. Kansal, CeO_2/ZnO hexagonal nanodisks: efficient material for the degradation of direct blue 15 dye and its simulated dye bath effluent under solar light, J. Alloys Compd. 620 (2015) 67–73.
[6] C. Wang, M.H. Cao, P.F. Wang, Y.H. Ao, Preparation, characterization of CdS-deposited graphene–carbon nanotubes hybrid photocatalysts with enhanced photocatalytic activity, Mater. Lett. 108 (2013) 336–339.
[7] Z.F. Liu, Z.G. Zhao, M. Miyauchi, Efficient visible light active $CaFe_2O_4/WO_3$ based composite photocatalysts: effect of interfacial modification, J. Phy. Chem. C 113 (39) (2009) 17132–17137.
[8] J.J. Xu, M.D. Chen, D.G. Fu, Study on highly visible light active Bi-doped TiO_2 composite hollow sphere, Appl. Surf. Sci. 257 (17) (2011) 7381–7386.
[9] M.H. Cao, P.F. Wang, Y.H. Ao, C. Wang, J. Hou, J. Qian, Photocatalytic degradation of tetrabromobisphenol A by a magnetically separable graphene–TiO_2 composite photocatalyst: mechanism and intermediates analysis, Chem. Eng. J. 264 (2015) 113–124.
[10] H. Jeong, T. Kim, D. Kim, K. Kim, Hydrogen production by the photocatalytic overall water splitting on NiO/$Sr_3Ti_2O_7$: effect of preparation method, Int. J. Hydrogen Energy 31 (9) (2006) 1142–1146.
[11] R. Abe, M. Higashi, K. Sayama, Y. Abe, H. Sugihara, Photocatalytic activity of R_3MO_7 and $R_2Ti_2O_7$ (R = Y: Gd, La; M = Nb, Ta) for water splitting into H_2 and O_2, J. Phys. Chem. B 110 (5) (2006) 2219–2226.
[12] Z.L. Hua, X. Zhang, X. Bai, L.L. Lv, Z. Ye, X. Huang, Nitrogen-doped perovskite-type $La_2Ti_2O_7$ decorated on graphene composites exhibiting efficient photocatalytic activity toward bisphenol A in water, J. Colloid Interface Sci. 450 (2015) 45–53.
[13] K.W. Li, Y. Wang, H. Wang, M.K. Zhu, H. Yan, Hydrothermal synthesis and photocatalytic properties of layered $La_2Ti_2O_7$ nanosheets, Nanotechnology 17 (19) (2006) 4863–4867.
[14] L.Q. Yang, S.Z. Kang, C. Hong, W.B. Bu, M. Jin, $La_2Ti_2O_7$: an efficient and stable photocatalyst for the photoreduction of Cr(VI) ions in water, Desalination 266 (1) (2011) 149–153.
[15] K. Onozuka, Y. Kawakami, H. Imai, T. Yokoi, T. Tatsumi, J.N. Kondo, Perovskite-type $La_2Ti_2O_7$ mesoporous photocatalyst, J. Solid State Chem. 192 (2012) 87–92.
[16] Z. Wang, K. Teramura, S. Hosokawa, T. Tanaka, Photocatalytic conversion of CO_2 in water over Ag-modified $La_2Ti_2O_7$, Appl. Catal. B Environ. 163 (2015) 241–247.
[17] C.H. Wu, Y.Z. Zhang, S. Li, H.J. Zheng, H. Wang, J.B. Liu, et al., Synthesis and photocatalytic properties of the graphene–$La_2Ti_2O_7$ nanocomposites, Chem. Eng. J. 178 (24) (2011) 468–474.
[18] Y.H. Ao, L.Y. Xu, P.F. Wang, C. Wang, J. Hou, J. Qian, Preparation of CdS nanoparticle loaded flower-like $Bi_2O_2CO_3$ heterojunction photocatalysts with enhanced visible light photocatalytic activity, Dalton Trans. 44 (25) (2015) 11321–11330.
[19] H.L. Wang, S.J. Li, L.S. Zhang, Z.G. Chen, J.Q. Hu, R.J. Zou, et al., Surface decoration of Bi_2WO_6 superstructures with Bi_2O_3 nanoparticles: an efficient method to improve visible-light-driven photocatalytic activity, CrystEngCommun 15 (2013) 9011–9019.
[20] S.S. Lee, H.W. Bai, Z.Y. Liu, D.D. Sun, Optimization and an insightful properties—activity study of electrospun TiO_2/CuO composite nanofibers for efficient photocatalytic H_2 generation, Appl. Catal. B Environ. 140–141 (2) (2013) 68–81.
[21] X.C. Meng, Z.S. Zhang, Facile synthesis of BiOBr/Bi_2WO_6 heterojunction semiconductors with high visible-light-driven photocatalytic activity, J. Photochem. Photobiol. A 310 (2015) 33–44.
[22] W.J. An, W.Q. Cui, Y.H. Liang, J.S. Hu, L. Liu, Surface decoration of $BiPO_4$ with BiOBr nanoflakes to build heterostructure photocatalysts with enhanced photocatalytic activity, Appl. Surf. Sci. 351 (2015) 1131–1139.
[23] H.Z. An, Y. Du, T.M. Wang, C. Wang, W.C. Hao, J.Y. Zhang, Photocatalytic properties of BiOX (X = Cl: Br, and I), Rare Met. 27 (3) (2008) 243–250.
[24] W.Q. Cui, W.J. An, L. Liu, J.S. Hu, Y.H. Liang, A novel nano-sized BiOBr decorated $K_2La_2Ti_3O_{10}$ with enhanced photocatalytic properties under visible light, J. Solid State Chem. 215 (2014) 94–101.
[25] S.J. Hu, B. Chi, J. Pu, J. Li, Novel heterojunction photocatalysts based on lanthanum titanate nanosheets and indium oxide nanoparticles with enhanced photocatalytic hydrogen production activity, J. Mater. Chem. A 2 (45) (2014) 19260–19267.
[26] X.C. Meng, Z.S. Zhang, Facile synthesis of BiOBr/Bi_2WO_6 heterojunction semiconductors with high visible-light-driven photocatalytic activity, J. Photochem. Photobiol. A 310 (2015) 33–44.
[27] Y.C. Miao, H.B. Yin, P. Peng, Y.N. Huo, H.X. Li, BiOBr/Bi_2MoO_6 composite in flower-like microspheres with enhanced photocatalytic activity under visible-light irradiation, RSC Adv. 6 (2016) 13498–13504.
[28] J. Cao, B.Y. Xu, H.L. Lin, S.F. Chen, Highly improved visible light photocatalytic activity of $BiPO_4$ through fabricating a novel p–n heterojunction BiOI/$BiPO_4$ nanocomposite, Chem. Eng. J. 228 (2013) 482–488.
[29] X.P. Lin, F.Q. Huang, J.C. Xing, W.D. Wang, F.F. Xu, Heterojunction semiconductor SnO_2/$SrNb_2O_6$ with an enhanced photocatalytic activity: the significance of chemically bonded interface, Acta Mater. 56 (12) (2008) 2699–2705.
[30] A. Nashim, K. Parida, n-$La_2Ti_2O_7$/p-$LaCrO_3$: a novel heterojunction based composite photocatalyst with enhanced photoactivity towards hydrogen production, J. Mater. Chem. A (2) (2014) 18405–18412.
[31] Y.N. Huo, X.F. Chen, J. Zhang, G.F. Pan, J.P. Jia, H.X. Li, Ordered macroporous Bi_2O_3/TiO_2 film coated on a rotating disk with enhanced photocatalytic activity under visible irradiation, Appl. Catal. B Environ. 148 (2014) 550–556.
[32] G.S. Gong, Q. Yang, Z. Gebru, Y.J. Fang, C.Y. Yin, C.M. Zhu, et al., Multiferroic properties in transition metals doped $La_2Ti_2O_7$ ceramics, J. Alloys. Compd. 611 (2014) 30–33.
[33] X.J. Wang, W.Y. Yang, F.T. Li, J. Zhao, R.H. Liu, S.J. Liu, et al., Construction of amorphous TiO_2/BiOBr heterojunctions via facets coupling for enhanced photocatalytic activity, J. Hazard. Mater. 292 (2015) 126–136.
[34] W.R. Zhao, Y. Wang, Y. Yang, J. Tang, Y.N. Yang, Carbon spheres supported visible-light-driven CuO-$BiVO_4$ heterojunction: preparation, characterization, and photocatalytic properties, Appl. Catal. B Environ. 115–116 (2012) 90–99.

[35] D.F. Sun, Y.D. Han, S. Gao, X.L. Zhang, Surface modification of titania-coated cobalt ferrite magnetic photocatalyst by cold plasma, Surf. Coat. Technol. 228 (9) (2013) 516–519.
[36] R. Wang, D. Xu, J.B. Liu, K.W. Li, H. Wang, Preparation and photocatalytic properties of CdS/$La_2Ti_2O_7$ nanocomposites under visible light, Chem. Eng. J. 168 (1) (2011) 455–460.
[37] K.K. Manga, Y. Zhou, Y. Yan, K.P. Loh, Multilayer hybrid films consisting of alternating graphene and titania nanosheets with ultrafast electron transfer and photoconversion properties, Adv. Funct. Mater. 19 (2009) 3638–3644.
[38] Y.S. Xu, W.D. Zhang, Anion exchange strategy for construction of sesame-biscuit-like $Bi_2O_2CO_3$/Bi_2MoO_6 nanocomposites with enhanced photocatalytic activity, Appl. Catal. B Environ. 140–141 (2013) 306–316.
[39] E.K. Heidari, A. Ataiea, M.H. Sohi, J.K. Kim, $NiFe_2O_4$/graphene nanocomposites with tunable magnetic properties, J. Magn. Magn. Mater. 379 (2015) 95–101.
[40] J.J. Xu, M.M. Wu, M.D. Chen, Z.M. Wang, A one-step method for fabrication of $CdMoO_4$–graphene composite photocatalyst and their enhanced photocatalytic properties, Powder Technol. 281 (2015) 167–172.
[41] J. Di, J.X. Xia, Y.P. Ge, H.P. Li, H.Y. Ji, H. Xu, Novel visible-light-driven CQDs/Bi_2WO_6 hybrid materials with enhanced photocatalytic activity toward organic pollutants degradation and mechanism insight, Appl. Catal. B Environ. 168 (2015) 51–61.
[42] J. Di, J.X. Xia, Y.P. Ge, H.P. Li, H.Y. Ji, H. Xu, The synergistic role of carbon quantum dots for the improved photocatalytic performance of Bi_2MoO_6, Nanoscale 7 (2015) 11433–11444.
[43] J.G. Hou, Z. Wang, S.Q. Jiao, H.M. Zhu, Bi_2O_3 quantum-dot decorated nitrogen-doped Bi_3NbO_7 nanosheets: in situ synthesis and enhanced visible-light photocatalytic activity, Cryst. Eng. Commun. 14 (18) (2012) 5923–5928.
[44] W.J. Li, D.Z. Li, J.X. Wang, Y. Shao, J.M. You, F. Teng, Exploration of the active species in the photocatalytic degradation of methyl orange under UV light irradiation, J. Mol. Catal. A Chem. 380 (2013) 10–17.
[45] J.X. Xia, J. Di, H.T. Li, H. Xua, H.M. Li, S.J. Guo, Ionic liquid-induced strategy for carbon quantum dots/BiOX(X = Br, Cl) hybrid nanosheets with superior visible light-driven photocatalysis, Appl. Catal. B Environ. 181 (2016) 260–269.
[46] J.X. Xia, J. Di, S. Yin, H. Xu, J. Zhang, L. Xu, H.M. Li, M.X. Ji, Y. Xu, Facile fabrication of the visible-light driven Bi_2WO_6/BiOBr composite with enhanced photocatalytic activity, RSC Adv. 4 (2014) 82–90.
[47] Y.R. Jiang, S.Y. Chou, J.L. Chang, S.T. Huang, H.P. Lin, C.C. Chen, Hydrothermal synthesis of bismuth oxybromide–bismuth oxyiodide composites with high visible light photocatalytic performance for the degradation of CV and phenol, RSC Adv. 5 (2015) 30851–30860.
[48] D. Zhang, J. Li, Q.G. Wang, Q.S. Wu, High {001} facets dominated BiOBr lamellas: facile hydrolysis preparation and selective visible-light photocatalytic activity, J. Mater. Chem. A 1 (2013) 8622–8629.
[49] D.F. Sun, Y.D. Han, S. Gao, X.L. Zhang, Surface modification of titania-coated cobalt ferrite magnetic photocatalyst by cold plasma, Surf. Coat. Technol. 228 (9) (2013) S516–S519.
[50] P.F. Wang, Y.H. Ao, C. Wang, J. Hou, J. Qian, Enhanced photoelectrocatalytic activity for dye degradation by graphene-titania composite film electrodes, J. Hazard. Mater. 223–224 (2012) 79–83.
[51] N. Zhang, Y.J. Xu, Aggregation and leaching-resistant: reusable, and multifunctional Pd@CeO_2 as a robust nanocatalyst achieved by a hollow core–shell strategy, Chem. Mater 25 (9) (2013) 1979–1988.
[52] Q.X. Xiang, J. Yu, M. Jaroniec, Synergetic Effect of MoS_2 and graphene as cocatalysts for enhanced photocatalytic H_2 production activity of TiO_2 nanoparticles, J. Am. Chem. Soc. 134 (15) (2012) 6575–6578.
[53] Y.X. Yu, W.X. Ouyang, W.D. Zhang, Photoelectrochemical property of the BiOBr-BiOI/ZnO heterostructures with tunable bandgap, J. Solid State Electrochem. 18 (2014) 1743–1750.
[54] N.T. Hahn, S. Hoang, J. Self, C. Buddie Mullins, Spray pyrolysis deposition and photoelectrochemical properties of n-type BiOI nanoplatelet thin films, ACS Nano 6 (2012) 7712–7722.
[55] D.L. Jiang, L.J. Men, J.X. Wang, Y. Zhang, C. Sara, Y.S. Wang, Redox reactions of copper complexes formed with different beta-amyloid peptides and their neuropathological relevance, Biochemistry 46 (2007) 9270–9282.
[56] Y.H. Zhang, N. Zhang, Z.R. Tang, Y.J. Xu, A unique silk mat-like structured Pd/CeO_2 as an efficient visible light photocatalyst for green organic transformation in water, ACS Sustain. Chem. Eng. 1 (10) (2013) 1258–1266.
[57] J. Xu, W. Meng, Y. Zhang, L. Li, C.S. Guo, Photocatalytic degradation of tetrabromobisphenol A by mesoporous BiOBr: efficacy, products and pathway, Appl. Catal. B 107 (107) (2011) 355–362.
[58] Q.C. Xu, D.V. Wellia, Y.H. Ning, R. Amal, T.T.Y. Tan, Synthesis of porous and visible-light absorbing Bi_2WO_6/TiO_2 heterojunction films with improved photoelectrochemical and photocatalytic performances, J. Phys. Chem. C 115 (15) (2011) 7419–7428.
[59] J. Shang, W.C. Hao, X.J. Lv, T.M. Wang, X.L. Wang, Y. Du, S.X. Dou, T.F. Xie, D.J. Wang, J.O. Wang, Bismuth Oxybromide with reasonable photocatalytic reduction activity under visible light, ACS Catal. 4 (2014) 954–961.
[60] J. Jiang, X. Zhang, P.B. Sun, L.Z. Zhang, ZnO/BiOI heterostructures: photoinduced charge-transfer property and enhanced visible-light photocatalytic activity, J. Phys. Chem. C 115 (42) (2011) 20555–20564.